

A possible electronic state quasi-half-valley-metal in VGe_2P_4 monolayer

San-Dong Guo¹, Yu-Ling Tao¹, Zhuo-Yan Zhao¹, Bing Wang², Guangzhao Wang³ and Xiaotian Wang⁴

¹*School of Electronic Engineering, Xi'an University of Posts and Telecommunications, Xi'an 710121, China*

²*Institute for Computational Materials Science, School of Physics and Electronics, Henan University, 475004, Kaifeng, China*

³*Key Laboratory of Extraordinary Bond Engineering and Advanced Materials Technology of Chongqing, School of Electronic Information Engineering, Yangtze Normal University, Chongqing 408100, China and*

⁴*Institute for Superconducting and Electronic Materials, University of Wollongong, Wollongong 2500, Australia*

One of the key problems in valleytronics is to realize valley polarization. Ferrovalley (FV) semiconductor and half-valley-metal (HVM) have been proposed, which possess intrinsic spontaneous valley polarization. Here, we propose the concept of quasi-half-valley-metal (QHVM), including electron and hole carriers with only a type of carriers being valley polarized. The QHVM may realize separation function of electron and hole. A concrete example of VGe_2P_4 monolayer is used to illustrate our proposal through the first-principle calculations. To better realize QHVM, the electric field is applied to tune related valley properties of VGe_2P_4 . Within considered electric field range, VGe_2P_4 is always ferromagnetic (FM) ground state, which possesses out-of-plane magnetization by calculating magnetic anisotropy energy (MAE) including magnetic shape anisotropy (MSA) and magnetocrystalline anisotropy (MCA) energies. These out-of-plane FM properties guarantee intrinsic spontaneous valley polarization in VGe_2P_4 . Within a certain range of electric field, the QHVM can be maintained, and the related polarization properties can be effectively tuned. Our works pave the way toward two-dimensional (2D) functional materials design of valleytronics.

Keywords: Valley, Electric field, Magnetic anisotropy

Email: sandongyuwang@163.com

I. INTRODUCTION

In analogy to charge/spin of electronics/spintronics, the valley has been recognized as an extra degree of freedom for carriers, widely known as valleytronics¹. The valley is characterized by a local energy extreme in the conduction band or valence band. In a material, two or more degenerate but inequivalent valley states should exist to encode, store and process information^{2,3}. For nonmagnetic valleytronic materials, 2H-transition-metal dichalcogenides (TMD) have attracted extensive attention⁴⁻¹⁰, because they have a pair of degenerate but inequivalent valleys and the large intervalley distance. However, these 2D materials lack spontaneous valley polarization. Although various strategies, such as optical pumping, magnetic field, magnetic substrates and magnetic doping⁴⁻¹⁰, have been executed to artificially induce valley polarization, these methods destroy the intrinsic energy band structures and crystal structures.

Fortunately, FV semiconductor with spontaneous spin and valley polarizations has been proposed¹¹, which breaks time-reversal and space-inversion symmetry with perfect coupling of the valley with charge and spin. The FV semiconductors have been predicted in many 2D materials¹¹⁻³⁰, which can overcome these shortcomings of the extrinsic valley polarization materials. Recently, in analogy to half-metals in spintronics (see Figure 1), the concept of HVM has been proposed³¹. The conduction electrons of HVM are intrinsically 100% valley polarized and 100% spin polarized even when including spin-orbit coupling (SOC). The electron correlation effect or strain can induce the FV semiconductor to HVM transition in some special 2D materials^{19,31-34}, which is generally related to topological phase transitions. How-

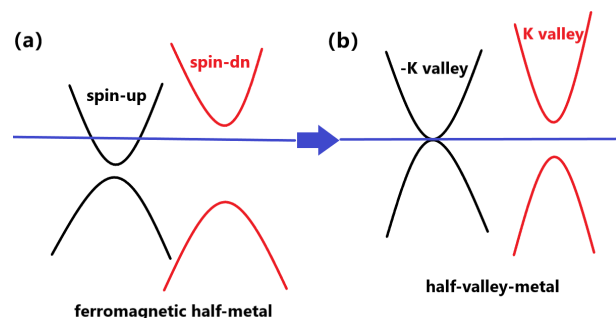


FIG. 1. (Color online) Schematic diagram of the analogy between ferromagnetic half-metal (a) and half-valley-metal (b). The spin-up/spin-dn is equivalent to -K/K valley. In (a), one spin channel is conducting, whereas the other is insulating. In (b), one valley channel is metal, in which conduction electrons are intrinsically 100% valley polarized, and the other is insulator.

ever, the HVM is just at one point, not a region of electron correlation strength or strain, which may be difficult to achieve in experiment.

In this work, we propose a concept of QHVM, where electron and hole carriers simultaneously exist with only a type of carrier being valley polarized (see Figure 2). In QHVM, the Fermi level slightly touches the conduction band minima (CBM) and valence band maxima (VBM), and the Berry curvature in 2D Brillouin zone (BZ) only occurs around -K and K valleys with opposite signs and unequal magnitudes. Under an in-plane longitudinal electric field E , the nonzero Berry curvature $\Omega(k)$ makes the carriers of -K valley obtain the general group velocity v_{\parallel} and the anomalous transverse velocity

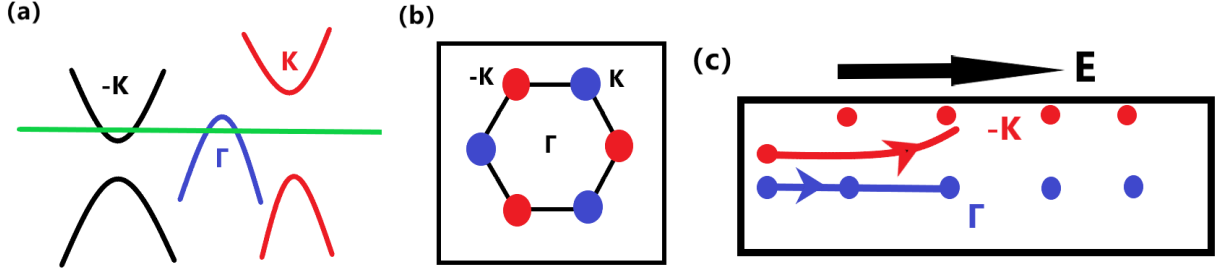


FIG. 2. (Color online) Schematic diagram of quasi-half-valley-metal: (a) the energy band structures, and the Fermi level slightly touches the CBM and VBM. (b): the distribution of Berry curvature in 2D BZ, and Berry curvature only occurs around -K and K valleys with opposite signs and unequal magnitudes. (c): under an in-plane longitudinal electric field E , the electronic carriers of -K valley turn towards one edge of the sample, and the hole carriers of Γ valley move in a straight line.

v_{\perp} ^{35,36}:

$$v = v_{\parallel} + v_{\perp} = \frac{1}{\hbar} \nabla_k \varepsilon(k) - \frac{e}{\hbar} E \times \Omega(k) \quad (1)$$

where v_{\parallel} (v_{\perp}) is along the electric field direction (perpendicular to the electric field and out-of-plane directions). However, carriers of Γ valley only obtain the general group velocity v_{\parallel} . The QHVM may be used to separate electron and hole carriers.

Recently, 2D MA_2Z_4 family with a septuple-atomic-layer structure has been established^{37,38} with diverse properties from common semiconductor to FV semiconductor to topological insulator to Ising superconductor, and MoSi_2N_4 and WSi_2N_4 of them have been achieved experimentally by the chemical vapor deposition method. Taking the VGe_2P_4 monolayer as an example, the QHVM can be realized by electric field. Within considered electric field range, the out-of-plane FM properties guarantee intrinsic spontaneous valley polarization in VGe_2P_4 . The QHVM can be maintained in a certain range of electric field, and the related polarization properties can be effectively tuned. Our findings may be extended to other FV semiconductors, and the QHVM can be achieved by electric field tuning.

The rest of the paper is organized as follows. In the next section, we shall give our computational details and methods. In the next few sections, we shall present structure and stabilities, magnetic anisotropy (MA) and electronic structures and electric field effects on physical properties of VGe_2P_4 monolayer. Finally, we shall give our discussion and conclusion.

II. COMPUTATIONAL DETAIL

Within density-functional theory (DFT)³⁹, the spin-polarized first-principles calculations are performed by employing the projected augmented wave method, as implemented in Vienna ab initio simulation package (VASP)^{40–42}. We use the generalized gradient approximation of Perdew-Burke-Ernzerhof (PBE-GGA)⁴³ as exchange-correlation functional. The on-site Coulomb correlation of V atoms is considered by the GGA+ U

method in terms of the on-site Coulomb interaction of $U = 3.0$ eV, as widely used in V-based MA_2Z_4 family^{18,20–22}. The GGA+ U adopts the rotationally invariant approach proposed by Dudarev et al⁴⁴, in which only the effective U (U_{eff}) based on the difference between the on-site Coulomb interaction parameter and exchange parameters is meaningful.

To attain accurate results, we use the energy cut-off of 500 eV, total energy convergence criterion of 10^{-8} eV and force convergence criteria of less than 0.0001 eV.Å⁻¹ on each atom. A vacuum space of more than 20 Å is used to avoid the interactions between the neighboring slabs. A Γ -centered $16 \times 16 \times 1$ k-point meshes in the BZ are used for these calculations of structure optimization, electronic structures and elastic constants, and a $9 \times 16 \times 1$ Monkhorst-Pack k-point meshes for calculating FM/antiferromagnetic (AFM) energy with rectangle supercell, as shown in FIG.1 of electronic supplementary information (ESI) along with the first BZ. The SOC effect is explicitly included to investigate MCA and electronic properties of VGe_2P_4 monolayer.

Through the direct supercell method, the interatomic force constants (IFCs) using GGA+ U are calculated with the $5 \times 5 \times 1$ supercell. Based on calculated harmonic IFCs, the phonon dispersions are obtained by using Phonopy code⁴⁵. The elastic stiffness tensor C_{ij} are carried out by using strain-stress relationship (SSR), and the 2D elastic coefficients C_{ij}^{2D} have been renormalized by $C_{ij}^{2D} = L_z C_{ij}^{3D}$, in which the L_z is the length of unit cell along z direction. The Berry curvatures are directly calculated from wave functions based on Fukui's method⁴⁶ by using VASPBERRY code^{47,48}.

III. STRUCTURE AND STABILITY

The crystal structures of VGe_2P_4 monolayer are shown in Figure 3. Different from experimentally synthesized MoSi_2N_4 with α_1 phase³⁷, the α_2 structure becomes favorable for VGe_2P_4 ³⁸. Despite this difference, both α_2 and α_1 structures lack inversion symmetry with a space group of $P6m2$ (No.187), which allows spontaneous val-

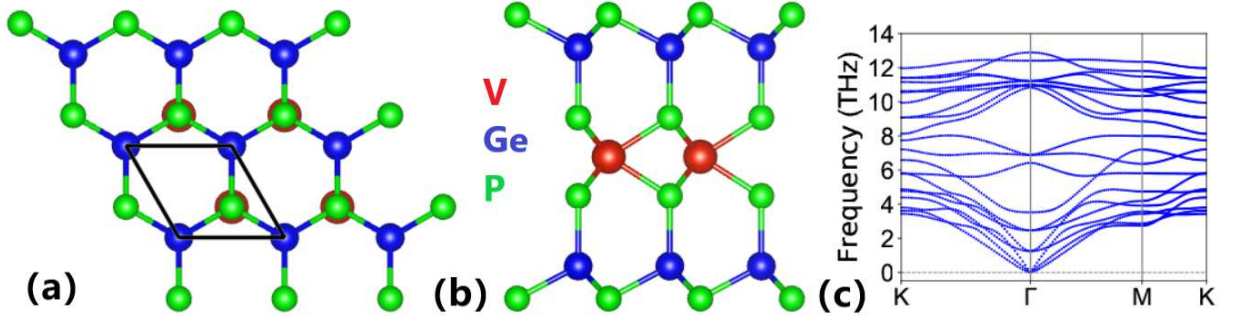


FIG. 3. (Color online) For VGe₂P₄ monolayer, (a): top view and (b): side view of crystal structure, and the primitive cell is shown by black lines in (a). (c): the phonon dispersions with FM order using GGA+*U* (*U* = 3 eV).

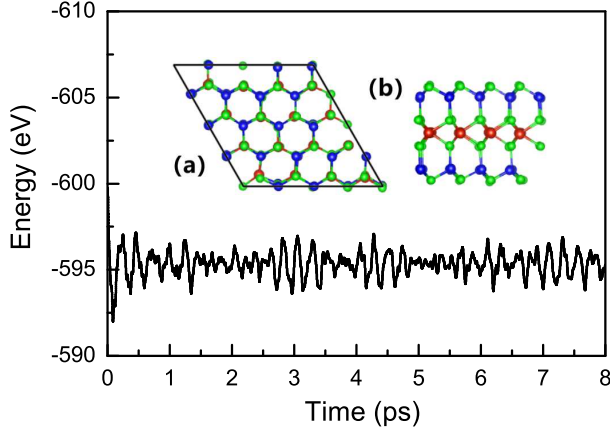


FIG. 4. (Color online) For VGe₂P₄ monolayer, the variation of free energy during the 8 ps AIMD simulation using GGA+*U* (*U* = 3 eV). Insets show the final structures (top view (a) and side view (b)) after 8 ps at 300 K.

ley polarization. The α_2 can be built by mirroring Ge₂P₂ double layers of α_1 with respect to the vertical surface. This crystal includes seven covalently bonded atomic layers in the order of P-Ge-P-V-P-Ge-P along the *z* axis. In other words, a MoS₂-like VP₂ layer is sandwiched between two slightly buckled honeycomb GeP layers. The optimized lattice constants *a* of VGe₂P₄ is 3.56 Å, which agrees well with previous theoretical value³⁸. To obtain the magnetic ground state, the total energy difference between AFM and FM ordering by using rectangle supercell (FIG.1 of ESI) is calculated, and VGe₂P₄ prefers FM state.

The dynamical stability of the VGe₂P₄ monolayer is proved by analyzing the phonon spectra, as shown in Figure 3. There are eighteen optical and three acoustical phonon branches, corresponding to a total of twenty-one branches due to seven atoms per cell. It is found that all phonon frequencies are positive in 2D BZ, confirming the dynamical stability of VGe₂P₄ at 0 K. Therefore, VGe₂P₄ can exist as a free-standing monolayer. From the application point of view, the mechanical stability of VGe₂P₄ is checked by elastic constants C_{ij} . Due to

hexagonal symmetry, the VGe₂P₄ has two independent elastic constants of C_{11} and C_{12} , and the calculated values are $C_{11}=182.68 \text{ Nm}^{-1}$ and $C_{12}=51.16 \text{ Nm}^{-1}$. These C_{ij} of VGe₂P₄ satisfy the Born criteria of mechanical stability ($C_{11} > 0$ and $C_{11} - C_{12} > 0$)⁴⁹, confirming its mechanical stability. The Ab initio molecular dynamics (AIMD) simulations are performed to assess the thermal stability of the VGe₂P₄ monolayer at room temperature. Figure 4 shows the free energy as a function of the simulation time, along with the snapshots of the geometric structure at the end of AIMD simulation at 300 K. The free energy is fluctuated around the equilibrium values without any sudden changes, and the small distortions in the final configuration are observed. This confirms the thermodynamical stability of VGe₂P₄ at room temperature, suggesting the possible room temperature applicability.

IV. MAGNETIC ANISOTROPY AND ELECTRONIC STRUCTURES

The magnetization of VGe₂P₄ can affect its symmetry. For out-of-plane FM state, all possible vertical mirror symmetry is broken, but the horizontal mirror symmetry is preserved, allowing the spontaneous valley polarization^{19,31–34}. The MAE can be used to decide the orientation of magnetization of VGe₂P₄. The negative/positive MAE means an easy axis along the in-plane/out-of-plane direction. The MAE mainly includes MCA energy E_{MCA} and MSA energy (E_{MSA}). The SOC can produce a link between the crystalline structure and the direction of the magnetic moments, giving rise to E_{MCA} . Based on GGA+*U*+SOC calculations, the E_{MCA} can be obtained by $E_{MCA} = E_{SOC}^{\parallel} - E_{SOC}^{\perp}$, where \parallel and \perp mean that spins lie in the plane and out-of-plane. Firstly, a collinear self-consistent calculation is performed to obtain the convergent charge density without SOC. Secondly, the convergent charge density is used to carry out noncollinear non-self-consistent calculation of two different magnetization directions (in-plane and out-of-plane) within SOC. The E_{MSA} is due to the

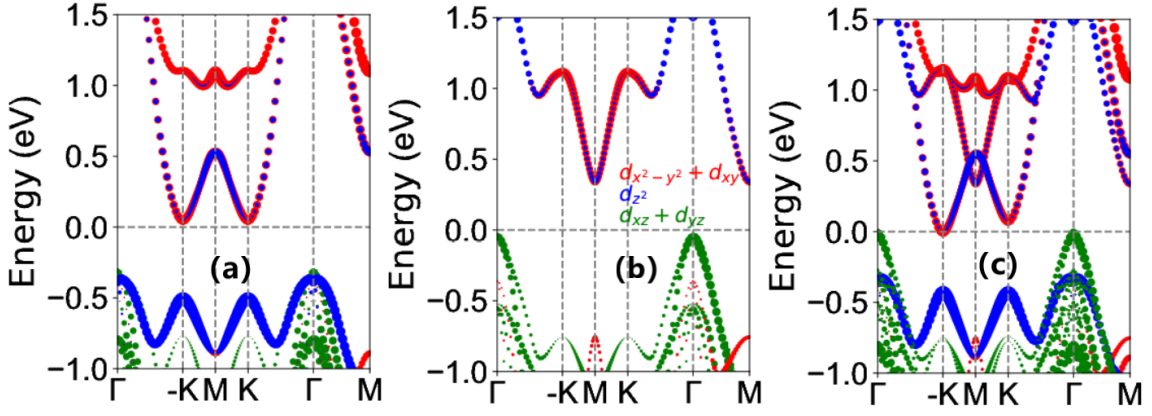


FIG. 5. (Color online) For VGe₂P₄ monolayer, the V- $d_{x^2-y^2}+d_{xy}$, d_{z^2} and $d_{xz}+d_{yz}$ -orbital characters energy band structures without SOC (a, b) and with SOC (c) using GGA+ U ($U=3$ eV). The (a) and (b) represent the band structure in the spin-up and spin-dn directions.

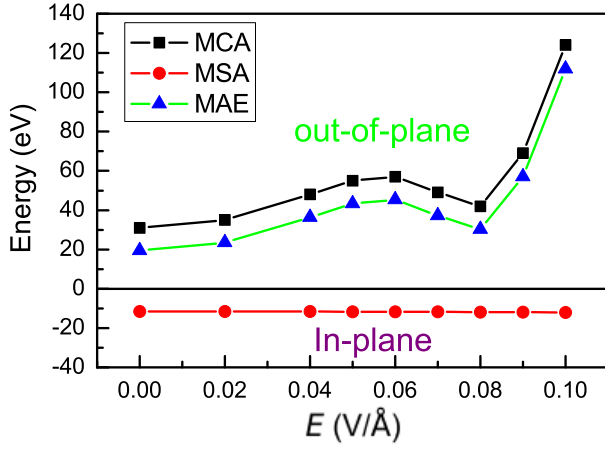


FIG. 6. (Color online) For VGe₂P₄ monolayer, the MCA energy, MSA energy and MAE as a function of E using GGA+ U ($U=3$ eV).

anisotropic dipole-dipole (D-D) interaction^{50,51}:

$$E_{D-D} = \frac{1}{2} \frac{\mu_0}{4\pi} \sum_{i \neq j} \frac{1}{r_{ij}^3} [\vec{M}_i \cdot \vec{M}_j - \frac{3}{r_{ij}^2} (\vec{M}_i \cdot \vec{r}_{ij})(\vec{M}_j \cdot \vec{r}_{ij})] \quad (2)$$

where the \vec{M}_i represent the local magnetic moments of V atoms, and vectors \vec{r}_{ij} connects the sites i and j .

For a collinear FM monolayer, the Equation 2 for in-plane case can be expressed as:

$$E_{D-D}^{\parallel} = \frac{1}{2} \frac{\mu_0 M^2}{4\pi} \sum_{i \neq j} \frac{1}{r_{ij}^3} [1 - 3 \cos^2 \theta_{ij}] \quad (3)$$

where θ_{ij} is the angle between the \vec{M} and \vec{r}_{ij} . For out-of-plane situation, the Equation 2 can further be simplified as:

$$E_{D-D}^{\perp} = \frac{1}{2} \frac{\mu_0 M^2}{4\pi} \sum_{i \neq j} \frac{1}{r_{ij}^3} \quad (4)$$

The E_{MSA} ($E_{D-D}^{\parallel} - E_{D-D}^{\perp}$) can be written as :

$$E_{MSA} = -\frac{3}{2} \frac{\mu_0 M^2}{4\pi} \sum_{i \neq j} \frac{1}{r_{ij}^3} \cos^2 \theta_{ij} \quad (5)$$

It is clearly seen that the crystal structure and local magnetic moment decide E_{MSA} . Generally, the MSA tends to make spins directed parallel to the monolayer.

For V-based MA₂Z₄, E_{MSA} has important effects on their magnetization direction^{17,52,53}. For VSi₂P₄ monolayer, an out-of-plane ferromagnet is predicted, when only E_{MCA} is considered¹⁸. However, the VSi₂P₄ will prefer in-plane case with including E_{MSA} ¹⁷. Calculated results show that VSi₂P₄ is a FV semiconductor for out-of-plane case using GGA+ U ($U=3$ eV), and it will become a common magnetic semiconductor for in-plane situation^{17,18}. So, the E_{MSA} is considered to decide magnetization direction of VGe₂P₄. Calculated results show that the MAE is 19 μ eV with E_{MCA} and E_{MSA} being 31 μ eV and -12 μ eV, and the positive MAE means that the easy magnetization axis of VGe₂P₄ is out-of-plane.

The spin-polarized band structures of monolayer VGe₂P₄ by using both GGA+ U and GGA+ U +SOC are calculated. In a trigonal prismatic crystal field environment, the V- d orbitals split into d_{z^2} orbital, $d_{xy}+d_{x^2-y^2}$ and $d_{xz}+d_{yz}$ orbitals, and these orbital characters energy band structures without SOC and with SOC are plotted in Figure 5. Based on Figure 5 (a) and (b), a distinct spin splitting can be observed due to the exchange interaction. It is found that VGe₂P₄ is an indirect band gap semiconductor of 0.091 eV, and its VBM and CBM are provided by the spin-dn and spin-up. The energies of -K and K valleys for both conduction and valence bands are degenerate, and no spontaneous valley polarization is observed.

The spontaneous valley polarization is induced by SOC. Calculated results show observable valley splitting between -K and K valleys in the conduction bands, and neglectful valley splitting in the valence bands. This dif-

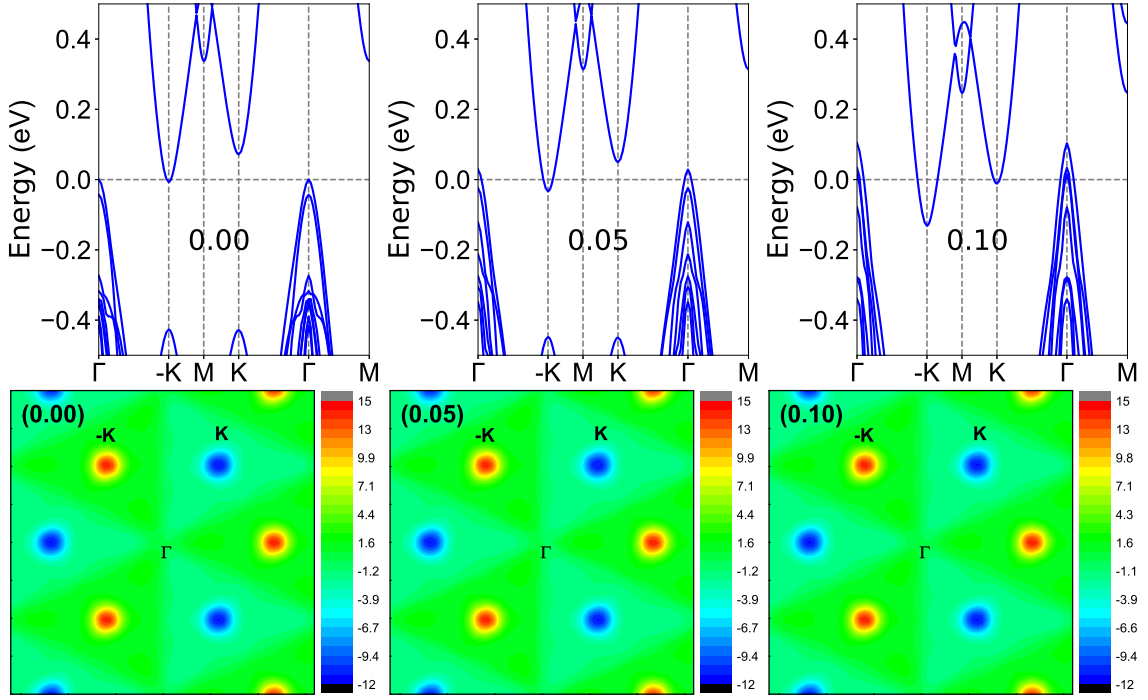


FIG. 7. (Color online) For VGe_2P_4 monolayer, the energy band structures (top) and distribution of Berry curvature in 2D BZ (bottom) at representative $E=0.00, 0.05$ and 0.10 V/Å using GGA+ U ($U = 3$ eV).

ference can be explained by the distribution of V- d orbitals. According to Figure 5, it is found that $d_{x^2-y^2}+d_{xy}$ orbitals dominate -K and K valleys of conduction bands, while the ones of valence bands are mainly from d_{z^2} orbitals. A simple perturbation theory can be used to further elucidate the essence of the valley polarization with SOC Hamiltonian of out-of-plane magnetization \hat{H}_{SOC}^0 ^{25,54}:

$$\hat{H}_{SOC}^0 = \alpha \hat{L}_z \quad (6)$$

in which \hat{L}_z and α are the orbital angular momentum along z direction and coupling strength. In light of the orbitals' contribution to -K and K valleys and their wave vector symmetry, the basis functions are chosen as:

$$|\phi_c^\tau\rangle = \sqrt{\frac{1}{2}}(|d_{x^2-y^2}\rangle + i\tau|d_{xy}\rangle) \quad (7)$$

$$|\phi_\nu^\tau\rangle = |d_{z^2}\rangle \quad (8)$$

where the subscript c , ν and τ represent conduction bands, valence bands and valley index ($\tau = \pm 1$). The energy levels at -K and K valleys are then defined as:

$$E^\tau = \langle \phi^\tau | \hat{H}_{SOC}^0 | \phi^\tau \rangle \quad (9)$$

According to the distribution of V- d orbitals, the valley splitting in the bottom conduction and top valence bands are given by^{25,54}:

$$|\Delta E^c| = E_c^K - E_c^{-K} = 4\alpha \quad (10)$$

$$|\Delta E^\nu| = E_\nu^K - E_\nu^{-K} = 0 \quad (11)$$

The perturbation theory results are in excellent consistency with the first-principle calculations.

According to Figure 5 (c), the VGe_2P_4 becomes a metal with a negative gap (G_{cv}) of -7 meV, when the SOC is included. The Fermi level slightly touches the CBM (-K valley) and VBM (Γ valley), but has no contact with K valley. Therefore, VGe_2P_4 monolayer is a QHVM. To describe properties of QHVM, two other gaps are defined. One is the Fermi level minus the energy of -K valley in the conduction bands (G_{-K}), which can describe concentration of electron carriers. Another is the energy of K valley in the conduction bands minus the Fermi level (G_K), which describes how easy the carriers of -K valley jump to K valley. The G_{-K} plus G_K equals to valley splitting in the conduction bands. For VGe_2P_4 , the G_{-K} is only about 7 meV, so it needs to be regulated through the external field, for example electric field.

V. ELECTRIC FIELD EFFECTS

Electric field can induce a semiconductor to metal transition in bilayer MoSi_2N_4 and WSi_2N_4 ⁵⁵. Moreover, the increasing electric field can result in a transition of MA from in-plane to out-of-plane in VSi_2P_4 ⁵⁶. In view of these facts, electric field may tune physical properties of QHVM in VGe_2P_4 . Firstly, we confirm the magnetic ground state under the electric field by the energy differences (per formula unit) between AFM and FM ordering,

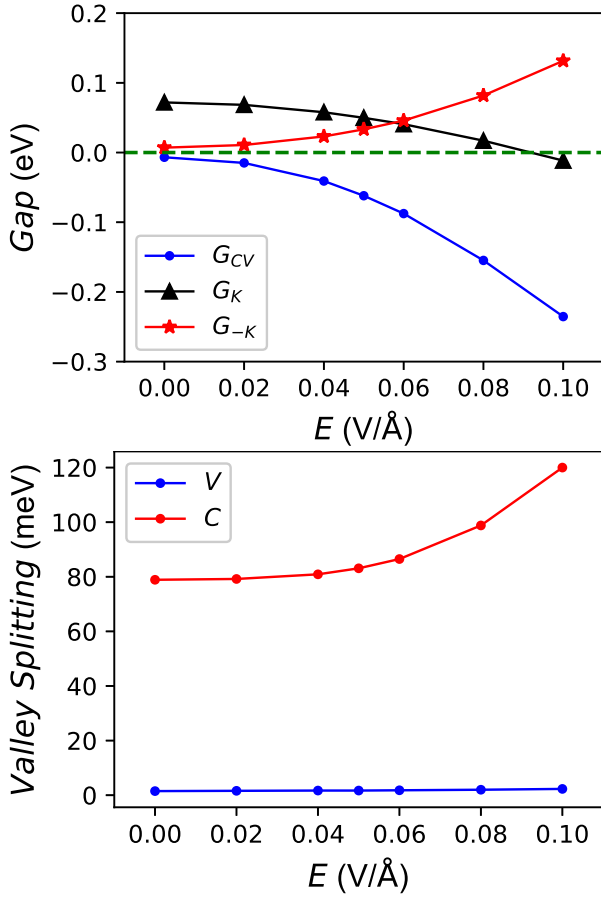


FIG. 8. (Color online) For VGe_2P_4 monolayer, the related band gap (top panel) and the valley splitting for both valence and conduction bands (bottom panel) as a function of E .

which are plotted in FIG.2 of ESI. Within considered E range, the FM ordering is always ground state. The MAE along with E_{MCA} and E_{MSA} as a function of E are plotted in Figure 6. It is found that the E_{MCA} is positive within considered E range, which firstly increases, then decreases, and then increases with increasing E . The E_{MSA} can be obtained by Equation 5. FIG.3 of ESI shows the local magnetic moment of V atom (M_V) as a function of E . It is found that the E has very little effects on M_V within considered E range, and the change is only $0.021 \mu_B$, which leads to the small change of E_{MSA} from $-11.58 \mu eV$ to $-12.03 \mu eV$. Finally, we calculate the MAE by $E_{MAE} = E_{MCA} + E_{MSA}$. It is clearly seen that E_{MAE} and E_{MCA} have the same trend with respect to E . In considered E range, E_{MAE} is always positive, implying that VGe_2P_4 possesses out-of-plane MA. This confirms spontaneous valley polarization in VGe_2P_4 within considered E range.

The energy band structures and Berry curvature distribution of VGe_2P_4 under electric field are investigated, and some representative ones are plotted in Figure 7. The evolutions of related gap (G_{cv} , G_{-K} and G_K) and valley splitting for both valence and conduction bands as a

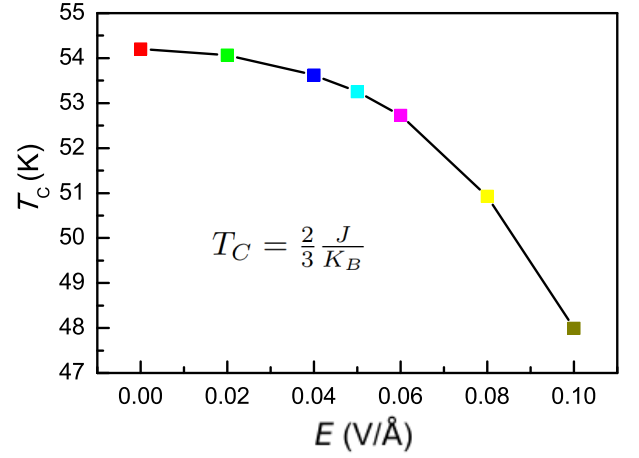


FIG. 9. (Color online) For VGe_2P_4 monolayer, the Curie temperature (T_C) as a function of E .

function of E are shown in Figure 8. With increasing E , the G_{-K} increases, which means that concentration of electron carriers increases. However, the G_K decreases, which means that the carriers of -K valley more easily jump to K valley. When $E > 0.09$ V/Å, the Fermi energy level simultaneously touches the -K and K valleys, and the QHVM will disappear. It is found that the increasing E can enhance valley splitting of conduction bands. So, the electric field can effectively tune physical properties of QHVM in VGe_2P_4 . By applying an in-plane longitudinal E in VGe_2P_4 , anomalous velocity v of Bloch electrons at -K valley is related with Berry curvature $\Omega(k)$ (see Figure 7): $v \sim E \times \Omega(k)$ ^{35,36}. The Berry curvature of -K valley forces the electron carriers to accumulate on one side of the sample, and the hole carriers of Γ valley move in a straight line. When an out-of-plane electric fields is applied, the carrier concentration can be effectively tuned.

To estimate Curie temperature T_C of VGe_2P_4 , it can be simply considered as a Ising spin system. The transition temperature can be expressed as $T_C = \frac{2}{3} \frac{J}{K_B}$ by using the mean-field approximations (MFA)⁵⁷, where J and K_B are the nearest-neighboring exchange parameter and Boltzmann constant, respectively. The J can be obtained from the energy difference between AFM (E_{AFM}) and FM (E_{FM}) orderings. According to the FM and AFM configurations, the E_{FM} and E_{AFM} can be written as:

$$E_{FM} = E_0 - 6JS^2 \quad (12)$$

$$E_{AFM} = E_0 + 2JS^2 \quad (13)$$

in which E_0 is the total energy of systems without magnetic coupling. The corresponding J can be attained:

$$J = \frac{E_{AFM} - E_{FM}}{8S^2} \quad (14)$$

The T_C vs E is plotted in Figure 9. Within E range, the predicted T_C is larger than 48 K.

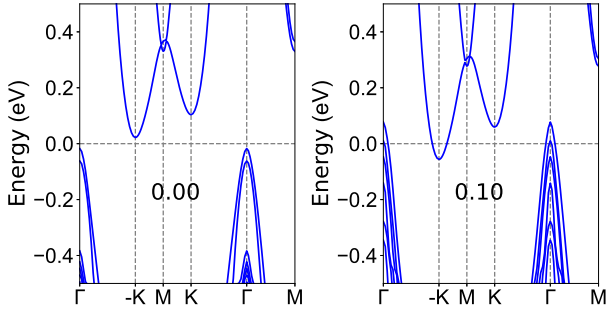


FIG. 10. (Color online) For VGe_2P_4 monolayer, the energy band structures at representative $E=0.00$ and 0.10 V/\AA using GGA+ U ($U = 4 \text{ eV}$).

VI. DISCUSSION AND CONCLUSION

For a given material, the correlation strength U should be determined from future experiment. Here, the $U=4 \text{ eV}$ is also used to investigate related properties of VGe_2P_4 to confirm that the QHVM can indeed be achieved by electric field tuning. FIG.4 of ESI shows that the FM ordering is ground state, when $E < 0.19 \text{ V/\AA}$. The E_{MAE} , E_{MCA} and E_{MSA} along with the local magnetic moment of V atom (M_V) as a function of E are plotted in FIG.5 and FIG.6 of ESI. When $E < 0.19 \text{ V/\AA}$, the positive E_{MAE} implies that VGe_2P_4 has out-of-plane MA. The evolutions of related gap (G_{cv} , G_{-K} and G_K) as a function of E are shown in FIG.7 of ESI. The representative energy band structures at $E=0.00$ and 0.10 V/\AA are plotted in Figure 10. Without electric field, VGe_2P_4 is a FV semiconductor with an indirect band

gap of 0.040 eV . The increasing E can induce FV semiconductor to QHVM transition with critical E of about 0.05 V/\AA . However, when $E > 0.15 \text{ V/\AA}$, the QHVM will disappear. For example $E=0.10 \text{ V/\AA}$, the VGe_2P_4 is a QHVM with G_{cv} , G_{-K} and G_K being -0.133 eV , 0.056 eV and 0.060 eV . When correlation strength U is in the reasonable range of 3 eV to 4 eV , the VGe_2P_4 can be tuned into QHVM by electric field.

In summary, we have proposed the concept of QHVM, which may be realized in monolayer VGe_2P_4 with dynamical, mechanical and thermal stabilities. The electric field can be used to tune the related physical properties of QHVM in VGe_2P_4 . For a certain electric field region, QHVM properties can be maintained, and the carrier concentration of -K valley can be effectively tuned. When in-plane and out-of-plane electric fields are applied, the electron carriers of -K valley transversely drift and eventually accumulate on one edge of the sample, while the hole carriers of Γ valley longitudinally move along the in-plane electric field direction. Our findings can inspire more works to search for QHVM.

Conflicts of interest

There are no conflicts to declare.

ACKNOWLEDGMENTS

This work is supported by Natural Science Basis Research Plan in Shaanxi Province of China (2021JM-456). We are grateful to Shanxi Supercomputing Center of China, and the calculations were performed on TianHe-2.

- ¹ J. R. Schaibley, H. Yu, G. Clark, P. Rivera, J. S. Ross, K. L. Seyler, W. Yao and X. Xu, Nat. Rev. Mater. **1**, 16055 (2016).
- ² L. J. Sham, S. J. Allen, A. Kamgar, and D. C. Tsui, Phys. Rev. Lett. **40**, 472 (1978).
- ³ S. A. Wolf, D. D. Awschalom, R. A. Buhrman, J. M. Daughton, S. von Molnár, M. L. Roukes, A. Y. Chtchelkanova, and D. M. Treger, Science **294**, 1488 (2001).
- ⁴ A. Srivastava, M. Sidler, A. V. Allain, D. S. Lembke, A. Kis, and A. Imamoglu, Nat. Phys. **11**, 141 (2015).
- ⁵ K. F. Mak, K. He, J. Shan, and T. F. Heinz, Nat. Nanotechnol. **7**, 494 (2012).
- ⁶ H. Zeng, J. Dai, W. Yao, D. Xiao, and X. Cui, Nat. Nanotechnol. **7**, 490 (2012).
- ⁷ H. Zeng, J. Dai, W. Yao, D. Xiao and X. Cui, Nat. Nanotechnol. **7**, 490 (2012).
- ⁸ M. Zeng, Y. Xiao, J. Liu, K. Yang and L. Fu, Chem. Rev. **118**, 6236 (2018).
- ⁹ C. Zhao, T. Norden, P. Zhang, P. Zhao, Y. Cheng, F. Sun, J. P. Parry, P. Taheri, J. Wang, Y. Yang, T. Scrase, K. Kang, S. Yang, G. Miao, R. Sabirianov, G. Kioseoglou, W. Huang, A. Petrou and H. Zeng, Nat. Nanotechnol. **12**, 757 (2017).
- ¹⁰ D. MacNeill, C. Heikes, K. F. Mak, Z. Anderson, A. Kormányos, V. Zólyomi, J. Park and D. C. Ralph, Phys. Rev. Lett. **114**, 037401 (2015).
- ¹¹ W. Y. Tong, S. J. Gong, X. Wan, and C. G. Duan, Nat. Commun. **7**, 13612 (2016).
- ¹² Y. B. Liu, T. Zhang, K. Y. Dou, W. H. Du, R. Peng, Y. Dai, B. B. Huang, and Y. D. Ma, J. Phys. Chem. Lett. **12**, 8341 (2021).
- ¹³ Z. Song, X. Sun, J. Zheng, F. Pan, Y. Hou, M.-H. Yung, J. Yang, and J. Lu, Nanoscale **10**, 13986 (2018).
- ¹⁴ J. Zhou, Y. P. Feng, and L. Shen, Phys. Rev. B **102**, 180407(R) (2020).
- ¹⁵ P. Zhao, Y. Ma, C. Lei, H. Wang, B. Huang, and Y. Dai, Appl. Phys. Lett. **115**, 261605 (2019).
- ¹⁶ S. D. Guo, J. X. Zhu, W. Q. Mu and B. G. Liu, Phys. Rev. B **104**, 224428 (2021).
- ¹⁷ S. D. Guo, Y. L. Tao, K. Cheng, B. Wang and Y. S. Ang, J. Phys.: Condens. Matter (2022). <https://doi.org/10.1088/1361-648X/ac9c3d>
- ¹⁸ X. Y. Feng, X. L. Xu, Z. L. He, R. Peng, Y. Dai, B. B. Huang and Y. D. Ma, Phys. Rev. B **104**, 075421 (2021).
- ¹⁹ S. Li, Q. Q. Wang, C. M. Zhang, P. Guo and S. A. Yang, Phys. Rev. B **104**, 085149 (2021).

- ²⁰ Q. R. Cui, Y. M. Zhu, J. H. Liang, P. Cui and H. X. Yang, Phys. Rev. B **103**, 085421 (2021).
- ²¹ Y. L. Wang and Y. Ding, Appl. Phys. Lett. **119**, 193101 (2021).
- ²² X. Zhou, R. Zhang, Z. Zhang, W. Feng, Y. Mokrousov and Y. Yao, npj Comput. Mater. **7**, 160 (2021).
- ²³ H. X. Cheng, J. Zhou, W. Ji, Y. N. Zhang and Y. P. Feng, Phys. Rev. B **103**, 125121 (2021).
- ²⁴ W. Du, Y. Ma, R. Peng, H. Wang, B. Huang, and Y. Dai, J. Mater. Chem. C **8**, 13220 (2020).
- ²⁵ R. Li, J. W. Jiang, W. B. Mi and H. L. Bai, Nanoscale **13**, 14807 (2021).
- ²⁶ K. Sheng, Q. Chen, H. K. Yuan and Z. Y. Wang, Phys. Rev. B **105**, 075304 (2022).
- ²⁷ P. Jiang, L. L. Kang, Y. L. Li, X. H. Zheng, Z. Zeng and S. Sanvito, Phys. Rev. B **104**, 035430 (2021).
- ²⁸ K. Sheng, H. K. Yuan and B. K. Zhang, Nanoscale (2022).DOI: 10.1039/d2nr03860a
- ²⁹ Y. Zang, Y. Ma, R. Peng, H. Wang, B. Huang, and Y. Dai, Nano Res. **14**, 834 (2021).
- ³⁰ R. Peng, Y. Ma, X. Xu, Z. He, B. Huang, and Y. Dai, Phys. Rev. B **102**, 035412 (2020).
- ³¹ H. Hu, W. Y. Tong, Y. H. Shen, X. Wan, and C. G. Duan, npj Comput. Mater. **6**, 129 (2020).
- ³² K. Sheng, B. K. Zhang, H. K. Yuan and Z. Y. Wang, Phys. Rev. B **105**, 195312 (2022).
- ³³ S. D. Guo, J. X. Zhu, M. Y. Yin and B. G. Liu, Phys. Rev. B **105**, 104416 (2022).
- ³⁴ S. D. Guo, W. Q. Mu and B. G. Liu, 2D Mater. **9**, 035011 (2022).
- ³⁵ X. Xu, W. Yao, D. Xiao and T. F. Heinz, Nat. Phys. **10**, 343 (2014).
- ³⁶ D. Xiao, M. C. Chang, and Q. Niu, Rev. Mod. Phys. **82**, 1959 (2010).
- ³⁷ Y. L. Hong, Z. B. Liu, L. Wang T. Y. Zhou, W. Ma, C. Xu, S. Feng, L. Chen, M. L. Chen, D. M. Sun, X. Q. Chen, H. M. Cheng and W. C. Ren, Science **369**, 670 (2020).
- ³⁸ L. Wang, Y. Shi, M. Liu, A. Zhang, Y.-L. Hong, R. Li, Q. Gao, M. Chen, W. Ren, H.-M. Cheng, Y. Li, and X.- Q. Chen, Nat. Commun. **12**, 2361 (2021).
- ³⁹ P. Hohenberg and W. Kohn, Phys. Rev. **136**, B864 (1964); W. Kohn and L. J. Sham, Phys. Rev. **140**, A1133 (1965).
- ⁴⁰ G. Kresse, J. Non-Cryst. Solids **193**, 222 (1995).
- ⁴¹ G. Kresse and J. Furthmüller, Comput. Mater. Sci. **6**, **15** (1996).
- ⁴² G. Kresse and D. Joubert, Phys. Rev. B **59**, 1758 (1999).
- ⁴³ J. P. Perdew, K. Burke and M. Ernzerhof, Phys. Rev. Lett. **77**, 3865 (1996).
- ⁴⁴ S. L. Dudarev, G. A. Botton, S. Y. Savrasov, C. J. Humphreys and A. P. Sutton, Phys. Rev. B **57**, 1505 (1998).
- ⁴⁵ A. Togo, F. Oba, and I. Tanaka, Phys. Rev. B **78**, 134106 (2008).
- ⁴⁶ T. Fukui, Y. Hatsugai and H. Suzuki, J. Phys. Soc. Japan. **74**, 1674 (2005).
- ⁴⁷ H. J. Kim, <https://github.com/Infant83/VASPBERRY>, (2018).
- ⁴⁸ H. J. Kim, C. Li, J. Feng, J.-H. Cho, and Z. Zhang, Phys. Rev. B **93**, 041404(R) (2016).
- ⁴⁹ E. Cadelano and L. Colombo, Phys. Rev. B **85**, 245434 (2012).
- ⁵⁰ X. B. Lu, R. X. Fei, L. H. Zhu and L. Yang, Nat. Commun. **11**, 4724 (2020).
- ⁵¹ K. Yang, G. Y. Wang, L. Liu , D. Lu and H. Wu, Phys. Rev. B **104**, 144416 (2021).
- ⁵² S. D. Guo, W.-Q. Mu, J.-H. Wang, Y.-X. Yang, B. Wang and Y.-S. Ang, Phys. Rev. B **106**, 064416 (2022).
- ⁵³ D. Dey, A. Ray and L. P. Yu, Phys. Rev. Materials **6**, L061002 (2022).
- ⁵⁴ P. Zhao, Y. Dai, H. Wang, B. B. Huang and Y. D. Ma, ChemPhysMater, **1**, 56 (2022).
- ⁵⁵ Q. Y. Wu, L. M. Cao, Y. S. Ang and L. K. Ang, Appl. Phys. Lett. **118**, 113102 (2021).
- ⁵⁶ S. D. Guo, X. S. Guo, G. Z. Wang, K. Cheng and Y. S. Ang, J. Mater. Chem. C (2022). <https://doi.org/10.1039/D2TC03293G>
- ⁵⁷ L. Ke, B. N. Harmon, and M. J. Kramer, Physical Review B **95**, 104427 (2017).